FIRST SUPERNOVAE IN DWARF PROTOGALAXIES

E.O. Vasiliev[1,2], E.I. Vorobyov[1,3], Yu.A. Shchekinov[4,5]

[1] Institute of Physics, Southern Federal University, Rostov-on-Don 344090 Russia, *eugstar@mail.ru*

[2] Institute of Astronomy, Russian Academy of Sciences, 119017 Moscow Russia

[3] Institute for Computational Astrophysics, Saint Mary's University, Halifax, B3H 3C3, Canada *vorobyov@ap.smu.ca*

[4] Department of Physics, Southern Federal University, Rostov-on-Don 344090 Russia, *yus@phys.rsu.ru*

[5] Special Astrophysical Observatory, Nizhny Arkhyz 369167 Russia

ABSTRACT. Using a two-dimensional hydrodynamics code with axial symmetry we explore the chemical, thermal, and dynamical evolution of a shell formed by a high-energy supernova explosion (10^{53} erg) in dwarf protogalaxies with a total (dark matter plus baryonic) mass 10^7 $M_\odot$ at a redshift $z = 12$. We consider two initial configurations for the baryonic matter, one without rotation and the other having the ratio of rotational to gravitational energy $\beta = 0.17$. The (non-rotating) dark matter halo is described by a quasi-isothermal sphere. We find that the dynamics of the shell is different in protogalaxies with and those without rotation. For instance, the Rayleigh-Taylor instability in the shell develops faster in protogalaxies without rotation. The fraction of a blown-away baryonic mass is approximately twice as high in models with rotation than in models without rotation. We argue that these differences are caused by different *initial* gas density profiles in non-rotating and rotating protogalaxies. On the other hand, the chemical evolution of gas in protogalaxies with and without rotation is found to be similar. The relative number densities of molecular hydrogen and HD molecules in the cold gas ($T \leq 10^3$ K) saturate at typical values of 10^{-3} and 10^{-7}, respectively. The clumps formed in the fragmented shell move with velocities that are at least twice as high as the escape velocity. The mass of the clumps is $\sim 0.1 - 10$ $M_\odot$, which is lower than the Jeans mass.

Key words: cosmology, galaxies, ISM, molecules, stars, shock waves.

1. Introduction

The detection of extremely metal-poor stars in our Galaxy with an iron abundance equal to or less than 10^{-3} of the solar value (Beers et al., 1992, Christlieb et al., 2002) has motivated scientists to put forward possible scenarios for the formation of such stars. According to Tsujimoto et al., (1999), extremely metal-poor (EMP) stars form in a dense shell produced by Type II supernova explosions of the first stars and accrete metals from the surrounding medium during the subsequent evolution. The formation of EMP stars is made possible by fragmentation of the primordial gas in a supernova shell due to efficient cooling by molecular hydrogen and HD molecules (see review by Nishi & Susa (1999), Salvaterra et al., (2004), Greif et al., (2007)). It now becomes evident that the formation of EMP stars due to fragmentation of supernova driven shells is a complicated phenomenon that depends on a variety of physical conditions in a host protogalaxy, which may vary from allowing star formation to shutting it off completely. In such circumstances, the construction of increasingly more sophisticated numerical models is justified. Here we perform axially symmetric numerical hydrodynamics simulations of high-energy supernova explosions (10^{53} erg) in a model dwarf protogalaxy with total mass 10^7 $M_\odot$. We seek to determine the effect of galactic rotation on the dynamical and chemical evolution of a supernova-driven shell.

2. Model protogalaxy

Our model protogalaxy consists of a baryonic component surrounded by a spherical dark matter halo. We assume that the dark matter halo profile is spherically symmetric and is determined by a modified isothermal sphere. The dark halo mass ($M_{\rm h}$) in our numerical simulations is set to 10^7 $M_\odot$, which, at a redshift of $z = 12$, corresponds to 3σ perturbations in the ΛCDM model for the parameters determined from the third

year WMAP data.[1] The virial radius of our model protogalaxy is $r_{\rm v} = 520$ pc (Ciardi & Ferrara 2004).

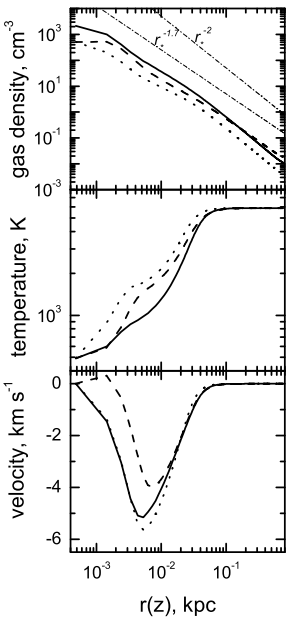

Figure 1: Profiles for the gas density (top panel), temperature (middle panel), and infall velocity (bottom panel) in the non-rotation model 1 (solid line) and rotating model 2 (dashed and dotted lines). In particular, the dashed and dotted lines show the radial and vertical profiles in model 2, respectively.

The initial distribution of the total gas density ($\rho_{\rm g}$) is found by solving numerically the steady-state momentum equations in cylindrical coordinates (z, r). We introduce a parameter $\beta < 1$, which is the ratio of rotational to gravitational energy. In the following text, we consider two models: model 1 without rotation, $\beta = 0$ and model 2 with rotation, for which we choose $\beta = 0.17$. The gas is assumed to be *initially* isothermal at a virial temperature $T_{\rm vir} = 5900$ K.

The dynamics of the gaseous component is followed by numerically solving a usual set of hydrodynamic equations in cylindrical coordinates (z, r, ϕ) using a finite-difference operator-split code (Stone & Norman 1992). The computational domain has a size of 750 pc in both the vertical (z) and horizontal (r) directions. The numerical resolution is 780×780 grid zones.

Once the equilibrium gas density distribution is constructed, we let our model galaxies evolve out of equilibrium. We stop this process when the temperature in the centre drops below 500 K. The resulted distributions are shown in Fig. 1. After we release 10^{53} erg of thermal energy in the central sphere with radius 5 pc. Such energetic supernovae are expected to result from explosion of massive metal-free stars (Heger & Woosley 2002).

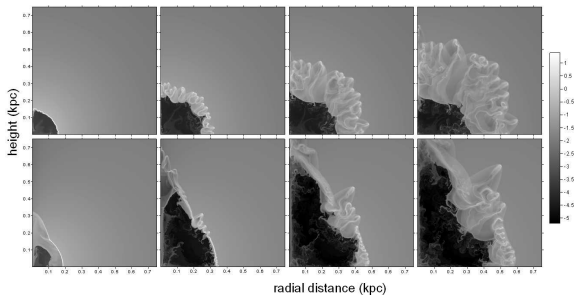

Figure 2: Distribution of density (in cm^{-3}) at t = 1, 4, 8, 12 Myr after SN explosion with $E_{SN} = 10^{53}$ erg in halo $M = 10^7\ M_\odot$ for the spin parameter $\beta = 0$ – *upper* and $\beta = 0.17$ – *low* row of panels.

The gas component of our model protogalaxy consists of a standard set of species: H, He, H^+, H^-, H_2, H_2^+, D, D^+, HD. The cooling rates are computed separately for temperatures below and above 2×10^4 K. In the low-temperature regime, the cooling rate includes cooling due to recombination and collisional excitation of atomic hydrogen (Cen 1992), H_2 (Galli & Palla 1998) and HD molecules (Lipovka et al., 2005). In the high-temperature regime, the cooling rates for zero metallicity are taken from (Sutherland & Dopita 1993). The list of chemical reactions and other details of solving chemical kinetics can be found in (Vasiliev et al 2008).

3. Results

Fig. 2 presents snapshots of the gas density distribution at four consecutive times after the supernova explosion. When the characteristic cooling time becomes shorter than the dynamical time (the age of a supernova remnant), an expanding shell becomes unstable to the Rayleigh-Taylor (RT) instability (Gull 1973). As a result, small ripples that distort a spherical shape of the shell appear in model 1 at $t = 1$ Myr. The subsequent evolution of the shell is governed by the RT instability, which acts mostly in the compressed gas of the shell outside the interface between hot supernova ejecta and the shell of compressed material. The characteristic time for the development of the RT instability is shorter for steeper initial gas density profiles and vice versa. Fig. 1 indicates that both the gas density distribution in model 1 and the *vertical* gas density distribution in model 2 have profiles similar to r_*^{-2}, where $r_* = (r^2 + z^2)^{1/2}$ is the distance from the galactic centre. On the other hand, the *radial* gas density distribution in model 2 is noticeably shallower and follows an $r_*^{-1.7}$ profile. Hence, we expect the RT instability to grow faster in the non-rotating model 1.

[1] We assume a ΛCDM cosmology with the parameters $(\Omega_0, \Omega_\Lambda, \Omega_m, \Omega_b, h) = (1.0,\ 0.76,\ 0.24,\ 0.041,\ 0.73)$, and deuterium abundance 2.78×10^{-5} (Spergel et al., 2007).

This is indeed seen in the top row of Fig. 2 – the shell has lost its spherical shape by $t = 4$ Myr and prominent spurs (or fingers) start to grow into the unperturbed medium. Model 2 shows little spurs at the same evolutionary time, though the shell has already started to show first signs of instability.

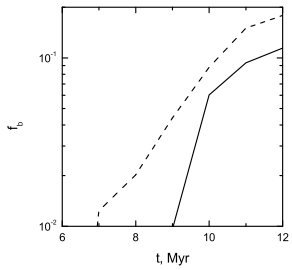

Figure 3: Fraction of the baryonic mass blown away by a supernova energy release of 10^{53} ergs in model 1 (solid) and in model 2 (dash).

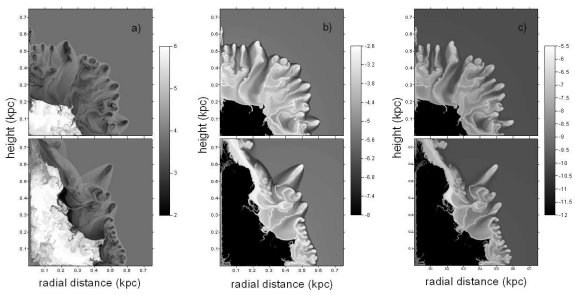

Figure 4: Logarithmic distribution of temperature (*left*), H_2 (*middle*) and HD (*right*) abundances at time $t = 12$ Myr after the explosion of SN with energy $E_{SN} = 10^{53}$ erg in halo with mass $M = 10^7\ M_\odot$ and the parameter $\beta = 0$ (upper) and $\beta = 0.17$ (lower).

Figure 2 shows that at $t = 12$ Myr some spurs are found outside the virial radius (520 pc) in the both models. This implies that a fraction of the baryonic mass is blown away by the supernova explosion (Fig. 3). We find that the spurs are characterized by mean mass-weighted velocities of the order of 26 km s^{-1} in model 1 and 22 km s^{-1} in model 2, whereas the escape velocity at the virial radius in both models is $v_e \approx 13$ km s^{-1}.

Fig. 4 shows the distribution of gas temperature, relative number densities of molecular hydrogen and HD molecules at $t = 12$ Myr. It is evident that low gas temperatures (below 10^3 K) are found in the shell and the spurs, where cooling takes place due to H_2 and HD molecules. In particular, the lowest temperatures found in the spur cores are of the order of 500 K and the relative number densities of H_2 and HD are approximately 10^{-3} and 10^{-7}, respectively.

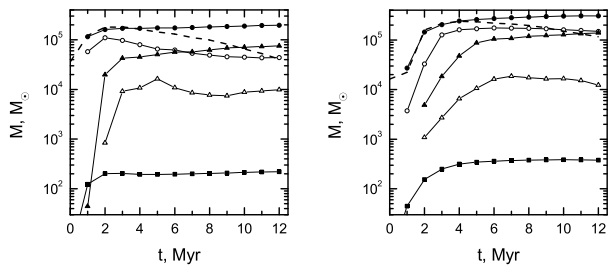

Figure 5: The total mass of gas in computational domain for model 1 with H_2 abundance higher than $x[H_2] = 5 \times 10^{-4}$ (filled circles), $x[H_2] = 10^{-3}$ (open circles), with temperature lower than $T \leq 10^3$ K (filled triangles), $T \leq 500$ K (open triagles). The line with filled squares represents the total H_2 mass. The dashed line shows the gas mass contained in fragments with density $\log n > -0.25$ and temperature $T < 5 \times 10^3$ K.

Figs. 5 present the temporal evolution of different molecular hydrogen tracers in model 1 and model 2. The comparison of those figures shows that the H_2 traces saturate during the evolution. The saturation is explained by the fact that we consider the gas evolution behind strong shock waves. The saturation times in model 2 are systematically longer than in model 1. This can be attributed to longer cooling times in model 2 due to a shallower initial gas density profile.

4. Evolution of fragments

One can see from Figs. 2 that the typical radial length of the most cold and dense regions is several parsecs. The clumps form due to desintegration of the shock wave under Rayleigh-Taylor instability which develops when gas behind the shock front starts cooling rapidly and the front decelerates. A typical size of fragments is expected to be close to the thickness of the compresses gas behind the front at the moment, when it becomes unstable.

Among possible mechanisms of cloud destruction stripping of the external layers of clouds seems the most efficient under the conditions of interest. This process operates mostly by Kelvin-Helmholtz instability. The stripping time for typical conditions in the case considered here equals ~ 3 Myr. This is short compared to the dynamical time, and from this point of view dense clumps should be destroyed quickly. However, the radiative cooling time is of the same order $t_c \sim 1 - 3$ Myr, which means that the density increase always connected with the radiative cooling can inhibite the destruction through stripping, so that the clumps can survive on longer dynamical time. The clumps however asymptotically are destroyed, which is seen from the fact that the mass contained in

relatively dense ($n > 0.56$ cm^{-3}) and cold ($T < 5 \times 10^3$ K) fragments decreases at $t > 3$ Myr as shown in Fig. 5 by dashed lines. Moreover, a typical mass of the most dense ($n > 1.8$ cm^{-3}) clumps $M \sim 0.1 - 10\ M_\odot$ (see Fig. 6) is much smaller than the Jeans mass for the corresponding conditions ($n \leq 1.8$ cm^{-3} and $T \sim 0.5 - 1 \times 10^3$ K). All this means that protostellar clouds do not form in the shell unless the clumps merge.

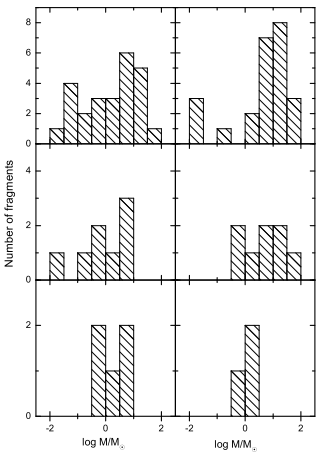

Figure 6: Number of fragments in the expanding shell at $t = 12$ Myr for a protogalaxy without (left) and with (right) rotation; panels from the uppermost to the lowermost correspond to the fragments with log $n > -0.25,\ 0,\ 0.25$, respectively; the mass of the fragments was calculated as $\bar{\rho} S^{3/2}$, where S is the area of a filamentary fragment on the "radius-height" plane, $\bar{\rho}$ is the mean density in it; note, the fragments of low density do look more filamentary and irregularly shaped than the dense ones, what therefore explains a higher spread of masses of fragments with lower density limit.

5. Conclusions

We have considered numerically the effect of energetic supernovae explosions (10^{53} erg) in non-rotating and rotating protogalaxies with the total mass $10^7\ M_\odot$ at a redshift of $z = 12$. We find the following:

- the process of the shell destruction is different for non-rotating and rotating protogalaxies;
- the supernova evacuates about 10% and 20% of the initial gas mass for models without and with rotation, respectively, to radial distances larger than the virial radius;
- the relative number densities of molecular hydrogen and HD molecules in the fingers and spurs are found to be quite large, approximately 10^{-3} and 10^{-7}, respectively. The typical temperature in the spur cores is of the order of 500 K at $t \geq 8$ Myr after the supernova explosion;
- the total gas mass with $x[\mathrm{H}_2] \geq 10^{-3}$ saturates at $2 \times 10^5\ M_\odot$, which corresponds to approximately 10% of the total baryonic mass in our model galaxy.

Finally, we would like to note that the typical masses of most fragments are $\sim 0.1 - 10\ M_\odot$. For the typical densities and temperatures in the fragments to be $\sim 0.5 - 1$ cm^{-3} and $(0.5 - 1) \times 10^3$ K, respectively, these masses are strongly sub-Jeans and the fragments are expected to be pressure-supported. Their further evolution depends on both the efficiency of cooling and destruction due to the Kelvin-Helmholtz instability. We do not expect that the low-mass stars can be formed in such conditions as suggested by Salvaterra et al. 2004. In our opinion, a more feasible mechanism for low-mass, metal-poor star formation is related with the re-collapse of a supernova bubble in protogalaxies, whose total gravitational binding energy is much larger than supernova energy.

Acknowledgements. We acknowledge Eugene Matvienko for his program of statistical processing. This work is supported by the RFBR grant 08-02-91321, the Federal Agency of Education grant RNP 2.1.1.3483. EOV is supported by the RFBR through the mobility programme grant 08-02-90706.

References

Beers T., Preston G., Shectman S.: 1992, *AJ*, **103**, 1987.
Burkert A.: 1995, *ApJ*, **447**, 25.
Cen R.: 1992, *ApJSS*, **78**, 341.
Ciardi B. & Ferrara A.: 2004, *SSR*, **116**, 625.
Christlieb N., Bessel M.S., Beers T.C., et al.: 2002, *Nature*, **419**, 904.
Galli D. & Palla F.: 1998, *A&A*, **335**, 403.
Greif T.H., Johnson J.L., Bromm V., Klessen R.S.: 2007, *ApJ*, **670**, 1.
Gull S.F.: 1973, *MNRAS*, **161**, 47.
Heger A. & Woosley S.E.: 2002, *ApJ*, **567**, 532.
Lipovka A., Núñez-López R., Avila-Reese V.: 2005, *MNRAS*, **361**, 850.
Nishi R. & Susa H.: 1999, *ApJ*, **523**, 103.
Salvaterra R., Ferrara A., Schneider R.: 2004, *NewA*, **10**, 113.
Spergel D.N., Bean R., Doré O. et al.: 2007, *ApJSS*, **170**, 377.
Stone J.M., Norman M.L.: 1992, *ApJSS*, **80**, 753.
Sutherland R. & Dopita M.: 1993, *ApJSS*, **88**, 253.
Tsujimoto T., Shigeyama T., Yoshii Y.: 1999, *ApJ*, **519**, 63.
Vasiliev E.O., Vorobyov E.I., Shchekinov Yu.A.: 2008, *A&A*, **489**, 505, arXiv/0807.3414.